Eu3+ Spectroscopy: A Structural Probe for Yttrium Orthoborate Phosphors

ARTICLE *in* THE JOURNAL OF PHYSICAL CHEMISTRY C · JANUARY 2010

Impact Factor: 4.77 · DOI: 10.1021/jp910329k

Eu^{3+} Spectroscopy: A Structural Probe for Yttrium Orthoborate Phosphors

Guohua Jia,[†] Peter A. Tanner,[†,*] Chang-Kui Duan,[‡] and Jeannette Dexpert-Ghys[§]

Department of Biology and Chemistry, City University of Hong Kong, Tat Chee Avenue, Kowloon, Hong Kong S.A.R., P. R. China, Institute of Modern Physics, Chongqing University of Post and Telecommunications, Chongqing 400065, P. R. China, and CEMES-CNRS, 29 rue Marvig BP 94347, 31055 Toulouse Cedex 4, France

Received: October 29, 2009; Revised Manuscript Received: January 8, 2010

Yttrium orthorborate YBO_3 containing 0.5 or 5 atom % of Eu^{3+} has been prepared by the spray-pyrolysis method. Low-temperature, high-resolution emission spectroscopy has been used to probe the local site symmetries of Eu^{3+} ions accommodated on the Y^{3+} sites in YBO_3:Eu^{3+} (0.5 atom %) and hence to determine the crystal structure of the title compound. The use of point group selection rules enabled a consistent spectral interpretation by envisaging distinct C_i and C_1 symmetry Eu^{3+} sites, in accordance with the neutron diffraction study of Lin et al. (*Chem. Mater.* **2004**, *16*, 2418). The assignment of features in the 10 K visible absorption spectrum of YBO_3:Eu^{3+} (5 atom %) is also consistent with the two-site model, but it was found that the site occupation by Eu^{3+} differs from the expected ratio $2C_1$:$1C_i$. The fitting of 31 crystal-field levels of the C_1 site has been made with some approximations by employing 7 parameters. In addition, the emission spectrum of YBO_3:Eu^{3+} containing a trace amount of Y_3BO_6 has been compared with those of YBO_3:Eu^{3+} and Y_3BO_6:Eu^{3+}, which serves as a reference to elucidate the concern on the red/orange color ratio of YBO_3:Eu^{3+} emission.

Introduction

There are many phases in the $Ln_2O_3-B_2O_3$ systems, including oxyborate Ln_3BO_6, orthoborate $LnBO_3$, and metaborate $Ln(BO_2)_3$. As Boyer et al.[1] pointed out, the lanthanide ion (Ln^{3+}) doped orthoborates YBO_3 and $GdBO_3$ are wide band gap materials which have received a great deal of attention recently due to their high UV transparency and exceptional optical damage threshold which allows them to withstand the harsh conditions present in vacuum discharge lamps and screens. In particular, these phosphors are attractive candidates for use in mercury-free lighting systems. Lanthanide orthoborates crystallize in several structures, including the aragonite, calcite, and pseudovaterite types.[2,3] Newnham et al.[4] noted that $LnBO_3$ compounds (Ln = La, Pr, Nd) are isomorphous with aragonite and the borates of smaller ions (e.g., Sc, In) crystallize in the calcite structure whereas the borates of Y and the lanthanides from Sm to Lu have the pseudovaterite structure, identified as the YBO_3 type. However, the YBO_3-type crystal structure has received much debate and various space groups have been proposed from previous crystallographic studies of related compounds[4–8] and will be referred to where relevant. We take the neutron diffraction study of $Y_{0.92}Er_{0.08}BO_3$ by Lin et al.[9] as the definitive crystal structure for the pseudovaterite lanthanide borates. This material crystallizes in the *C*2/*c* space group at both low (300 K) and high (1000 K) temperatures. The boron atoms were found to be tetrahedrally coordinated in $B_3O_9^{9-}$ groups at low temperature, whereas they are transformed into flat BO_3^{3-} triangles at high temperature. In the low-temperature polymorph, which is the system appropriate in the present study, the Y^{3+} ions are 8 coordinated but two bridging oxygens are quite distant. The approximate coordination environment of Y^{3+} is thus a trigonal antiprism (D_{3d}). Note that the ratio of $Y^{3+}(C_i)$ sites to $Y^{3+}(C_1)$ sites is 1:2. Figure 1 shows the nearest-neighbor coordination environments of the Y^{3+} ions at these two sites.

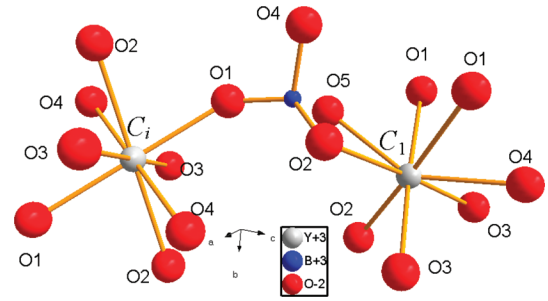

Figure 1. Nearest neighbor coordination environments of Y^{3+} in YBO_3 at the C_i and C_1 sites.[9]

There have been several previous reports of the emission spectra of YBO_3-type borates doped with Eu^{3+}, and the interpretations as well as the spectra themselves have differed considerably. As an aid to the reader, here and subsequently referred to, the number of spectral features expected for some $^5D_0$ emission transitions to ^7F_J multiplet terms are listed in Table 1 for Eu^{3+} ions located at sites of various point group symmetries. Note that the major intensity of the transition to $^7F_1$ is derived from the magnetic dipole mechanism, whereas transitions to other ^7F_J multiplets primarily derive intensity from the electric dipole mechanism and under the Judd formalism $\Delta J = 2$, 4, or 6 are allowed. Boyer et al.[1] compared the $^5D_0 \rightarrow {}^7F_1$ zero-phonon lines in the 14 K excitation spectra of YBO_3:Eu^{3+} samples prepared by a sol–gel method, a wet process, and the solid-state reaction. Three Gaussian bands were fitted, in each case, to bands between 17 202 and 17 215 cm^{-1}. However, the bands were at different locations for different samples, and this is not consistent with pure YBO_3:Eu^{3+}. In another publication of the same group,[10] three distinct Eu^{3+} sites were detected for samples of YBO_3:Eu^{3+} prepared by sol–gel

* To whom correspondence should be addressed. E-mail: bhtan@cityu.edu.hk.
† City University of Hong Kong.
‡ Chongqing University of Post and Telecommunications.
§ CEMES-CNRS.

10.1021/jp910329k
Published on Web 01/25/2010

TABLE 1: Number of Bands in Transitions from $^5D_0$ to ^7F_J ($J = 0-4$) for Some Different Site Symmetries of Eu^{3+}[a]

space group	symmetry of Y^{3+} sites
$P6_3/m$	$S_6 \equiv C_{3i}$
$R32$	C_1
$C2/c$	C_1 and C_i (ratio 2:1)
$P\bar{6}c2$	$3D_3$

	no. of bands in the $^5D_0 \rightarrow {}^7F_J$ transition				
site symmetry	$J = 0$ (ED)	$J = 1$ (MD)	$J = 2$ (ED)	$J = 3$ (ED)	$J = 4$ (ED)
C_{3i}	0	2	0	0	0
C_3	1	2	3	5	6
C_i	0	3	0	0	0
C_1	1	3	5	7	9
D_3	0	2	2	4	4

[a] The correspondence of Y^{3+} site symmetry to some proposed space groups of YBO_3 is also given. ED, electric dipole transition; MD, magnetic dipole transition.

and solid-state syntheses. Again, the $^7F_0 \rightarrow {}^5D_0$ excitation spectral bands were not coincident for the samples prepared by different methods. The 34 K emission spectra for a sample prepared by the sol−gel technique exhibited different emission bands for the $^5D_0 \rightarrow {}^7F_1$ transitions for different excitation lines. The results were interpreted in terms of the $P6_3/m$ space group (i.e., which implies the occupation of a single S_6 site by Eu^{3+}). Two intrinsic sites of C_3 symmetry were proposed to account for the spectra, in addition to a perturbed site, but there appear to be more than two $^5D_0 \rightarrow {}^7F_1$ transitions for each of the two C_3 sites (Figure 3 in ref 10). The 77 K spectrum of $LuBO_3$:Eu^{3+} between 570 and 640 nm was reported by Hölsa,[11] and it was in agreement with the 300 K spectrum of $GdBO_3$:Eu^{3+} previously reported by Bril and Wanmaker.[12] One band was observed for the $^5D_0 \rightarrow {}^7F_0$ transition and three for $^5D_0 \rightarrow {}^7F_1$ at one site of Eu^{3+}, whereas apparently only one band (for $^5D_0 \rightarrow {}^7F_1$) was attributed to a second site. Hölsa[11] concluded that the Eu^{3+} ions occupy D_{3d} and T sites in $LuBO_3$:Eu^{3+}, but this does not agree with any of the crystal structure determinations. In fact, the room-temperature spectra are not sufficiently well resolved to enable detailed spectral assignments to be made. Also, the more recent reports of the room-temperature emission spectra of YBO_3:Eu^{3+}[13] and (Y,Gd)BO_3:Eu^{3+}[14] are at low resolution so that the fine structure is not resolved. In another high-resolution room-temperature excitation spectrum of bulk YBO_3:Eu^{3+}, three $^5D_0 \rightarrow {}^7F_0$ zero-phonon lines are apparent (one main band at 580.9 nm with low- and high-energy shoulders: Figure 9 in ref 15), whereas the interpretation suggested the presence of only one Eu^{3+} site.

It is difficult to reconcile these results with the definitive crystal structure mentioned above. The locations of the zero-phonon lines differed for samples prepared by different methods and also when using different excitation lines. Finally, it is noted that none of the above low-temperature spectra of pseudovaterite phase YBO_3:Eu^{3+} are the same as those presented in this study. More detailed characterization work is therefore necessary, and in view of the conflicting spectral studies, the aim of the present work is to employ the spectroscopic probe Eu^{3+} in order to investigate the occurrence of different Eu^{3+} sites in the YBO_3 structure and to infer the site symmetry of each site. The low-temperature visible emission and absorption spectra of the phosphor YBO_3:Eu^{3+} have therefore been recorded and interpreted together with the results from other characterization methods. The partial energy level scheme of Eu^{3+} has been derived from the luminescence spectra, and a crystal-field fit has been made.

Experimental Section

The powder phosphor samples have been freshly prepared using a laboratory-scale spray-pyrolysis apparatus schematized in ref 16. The piezoelectric pellet frequency was 2.4 MHz, the air flow was maintained constant at 5 L min^{-1}, and the drying area was at the temperature of about 100 °C. For the preparation of the borate samples, a solution of the lanthanide nitrates in appropriate proportions and a solution of boric acid in water and methanol (10:1) were mixed. The solution was decomposed at 700 °C, and the obtained powder was further annealed at 1200 °C in air for 2 h. When the stoichiometric amount of H_3BO_3 (i.e., H_3BO_3:Y in the molar ratio of 1:1) was employed, the parasite phase Y_3BO_6 appeared. An excess of boric acid was therefore added systematically (1.2 times the stoichiometric amount), and the pure YBO_3 vaterite-type phase was obtained. Samples with the nominal concentrations of Eu^{3+} of 5 and 0.5 atom % were prepared. The pure oxyborate Y_3BO_6 was obtained by using the molar ratio Y:H_3BO_3 of 3:1, and this compound was also doped with Eu^{3+}.

Room-temperature FT-IR spectra of the samples in KBr discs were recorded between 400 and 4000 cm^{-1} at a resolution of 2 cm^{-1} using a Bomem MB-120 Spectrometer. X-ray powder diffraction (XRD) patterns were obtained by a Siemens D500 diffractometer using Cu Kα radiation ($\lambda = 1.54056$ Å) with a scanning rate of 1.2° min^{-1} in the angle range from 10° to 80°.

High-resolution emission spectra were recorded by using a tunable Panther OPO system pumped by the third harmonic of a Surelite Nd:YAG pulsed laser. The signal was collected at 90° with an Acton 0.5 m monochromator, having gratings with 1800, 1200, or 600 grooves mm^{-1}, blazed at 250, 500, or 750 nm, respectively, and a back-illuminated SpectruMM CCD detector. The powder sample was housed in an Oxford Instruments closed cycle cryostat with base temperature 10 K for all measurements. The setup of the absorption spectral measurements using compressed discs was the same as that employed for high-resolution emission, except that a tungsten lamp was employed as the light source. The samples did not exhibit any characteristics of a phase transition on cooling to 10 K, so that the Eu^{3+} site symmetry is taken as unchanged.

Results and Discussion

FT-IR Spectra. Laperches and Tarte[17] utilized IR spectra to distinguish between calcite-, aragonite-, and YBO_3-type borates. The distinction between the presence of triangular borate groups and tetrahedral coordination of boron can be made on this basis.[6,8,18] Basically, the presence of triangular BO_3^{3-} units is

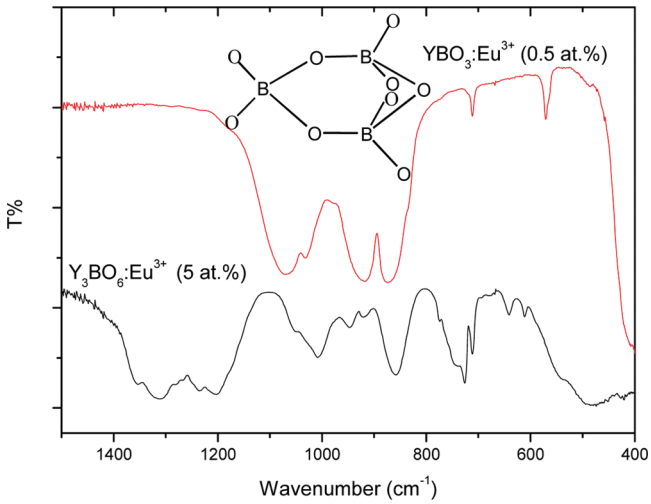

Figure 2. FT-IR spectra of YBO_3:Eu^{3+} (0.5 atom %) and Y_3BO_6:Eu^{3+} (5 atom %) between 400 and 1500 cm^{-1}. The schematic structure of the $B_3O_9^{9-}$ unit is also shown.

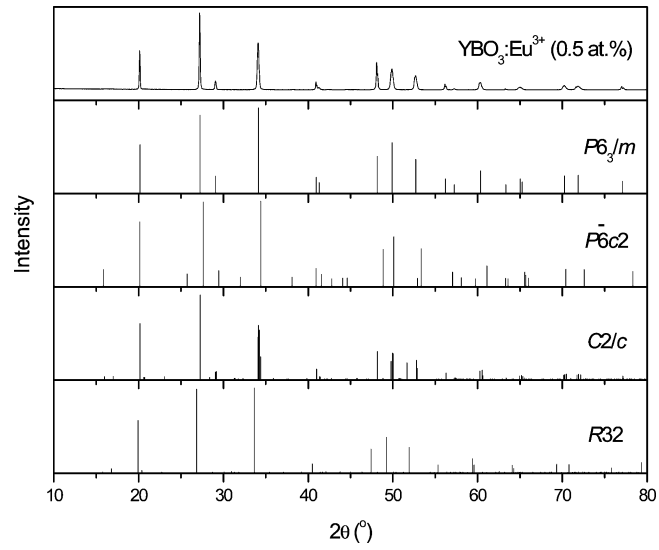

Figure 3. Comparison of the XRD pattern of YBO_3:Eu^{3+} (0.5 atom %) with standard files. The patterns for $P6_3/m$ (JCPDS: 88-0356), $P\bar{6}c2$ (JCPDS: 83-1205), $C2/c$ (JCPDS: 01-073-7388), and $R32$ (JCPDS: 89-6545) are given for reference.

characterized by strong bands at 1290 cm^{-1}, as in the infrared spectra of $LnBO_3$ (Ln = La, Pr),[19] whereas the presence of $B_3O_9^{9-}$ groups is marked by the absence of these features and other bands at ~900 cm^{-1}.

The FT-IR spectra of YBO_3:Eu^{3+} (0.5 atom %) and Y_3BO_6:Eu^{3+} (5 atom %) are shown in Figure 2. The former spectrum, with strong bands between 874 and 1071 cm^{-1}, is clearly indicative of $B_3O_9^{9-}$ groups in YBO_3, which is consistent with the crystal structure of Lin et al.[9] The bands at 874 and 920 cm^{-1} are due to ring stretching modes, whereas the peak at 1071 cm^{-1} is due to terminal B−O stretching. Assignments of bands in the FT-IR spectrum of Y_3BO_6:Eu^{3+} (5 atom %) have been made to the vibrational modes of triangular BO_3^{3-} and $B_2O_5^{4-}$ groups in which the boron atoms are all 3-fold coordinated, and the peak locations in Figure 2 agree well with those in the work performed by Lin and co-workers,[20] who interpreted the spectra of the oxyborate Y_3BO_6 (or which has been written as $Y_{17.33}(BO_3)_4(B_2O_5)_2O_{16}$[20]) in the *Cm* space group.

XRD. Figure 3 shows the XRD pattern of YBO_3:Eu^{3+} (0.5 atom %) together with four of the standard patterns proposed for the pseudovaterite structure. All patterns are similar with respect to the strongest six peaks. The peaks in $P\bar{6}c2$ (JCPDS: 83-1205) are shifted to about 0.5−0.6° higher than the pattern herein for the group between 48° and 53°. These shifts enabled the possibility that the compound may have crystallized in the $P\bar{6}c2$ space group to be excluded. It is not conclusive from our X-ray powder pattern whether the X-ray pattern corresponds to the $P6_3/m$, $R32$, or $C2/c$ space group. The results show that neutron diffraction is more discriminating in assigning the space group.

10 K High-Resolution Spectra of YBO_3:Eu^{3+}. The use of Eu^{3+} as a luminescence probe to distinguish between the possible site symmetry designations is now discussed. Assuming that Eu^{3+} occupies the Y^{3+} site in YBO_3 without any distortion of symmetry, then its site symmetry would be (i) C_{3i}, (ii) C_1, or (iii) C_i and C_1 in a 1:2 ratio, for the crystal space groups (i) $P6_3/m$, (ii) $R32$, or (iii) $C2/c$. It is also worth mentioning that for the space group $P\bar{6}c2$ the Eu^{3+} ions would occupy three distinct sites of D_3 symmetry. The local site symmetry of the Eu^{3+} ion can then be inferred from the number of bands in the transitions from $^5D_0$ to ^7F_J (J = 0−4) multiplet terms, as compared in Table 1.

The emission spectra of the samples with two different concentrations of Eu^{3+} were similar, with the difference that the bands in YBO_3:Eu^{3+} (5 atom %) were inhomogeneously broadened. Therefore, only YBO_3:Eu^{3+} (0.5 atom %) was subjected to detailed high-resolution emission spectral investigation since the local site symmetry of Eu^{3+} in this sample with lower dopant ion concentration suffers minimal distortion from that of the Y^{3+} site. Only the features in the $^5D_0 \rightarrow {}^7F_1$ transition showed significant differences when employing different laser excitation lines. Otherwise, the excitation wavelength-independent character and the number of observed features of the emission transitions $^5D_0 \rightarrow {}^7F_J$ (J = 0, 2, 3, and 4 with 1, 5, 6, and 7 bands resolved, respectively) showed that these transitions are associated exclusively with the occupation of one site with symmetry of a 2-fold axis or lower by Eu^{3+}. The nonobservation of the total number of expected bands for J = 3 and 4 is attributed to the weak intensity of spectral features. From the neutron diffraction study,[9] these bands are therefore associated with the C_1 site of Eu^{3+}.

The features in the $^5D_0 \rightarrow {}^7F_1$ emission transition are located in the range from 590.5 to 594.5 nm, and the intensities of these bands change considerably under different excitation laser lines, as depicted in Figure 4. In particular, the bands at highest energy are more strongly excited by higher energy laser lines. However, the relative intensities of the bands in the spectra with excitation by these wavelengths (marked as **1**−**4** in Figure 4) are only about 1/50 times as strong as the bands in the spectra using excitation by longer wavelengths (marked as **5**−**8** in Figure 4). The intensity ratios between the bands at 590.82, 591.97, and 594.0 nm and those at 592.67, 593.61, and 593.78 nm, however, are fixed rather than being excitation wavelength dependent, which clearly indicates that these two sets of bands represent the emission of Eu^{3+} from two different origins. We employed laser excitation into the $^5D_2$ multiplet term so that it was not possible to selectively excite one site. However, it is possible to derive the emission spectrum of a certain distinct site by selecting two spectra which employed different excitation lines and then normalizing on any one band contributed by only one site followed by the subtraction of one spectrum from the other. The derived spectra based upon the normalizations on the bands at 592.67 and 590.82 nm are shown in Figures 5 and 6, respectively. The subtraction of Figure 5a and 5b gives Figure 5c. Three bands are apparent for the $^5D_0 \rightarrow {}^7F_1$ transition, and

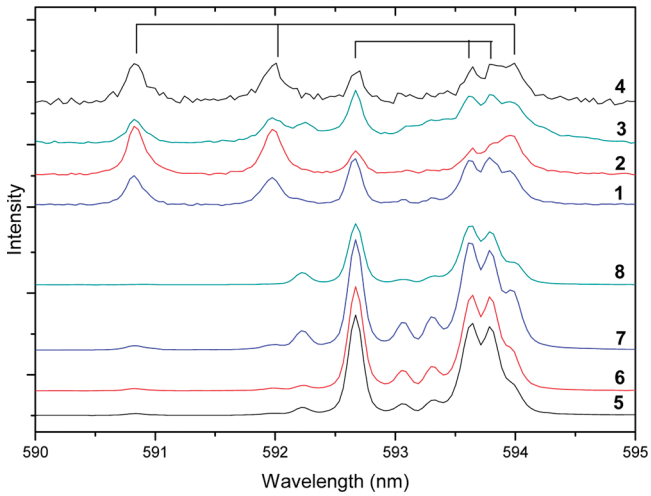

Figure 4. $^5D_0 \rightarrow {}^7F_1$ emission transition of YBO_3:Eu^{3+} (0.5 atom %) at 10 K on arbitrary scales excited by different laser lines (refer to the text). The excitation wavelengths in nm are marked on each spectrum: (1) 454.8, (2) 462.3, (3) 462.8, (4) 464.8, (5) 465.95, (6) 466, (7) 466.1, and (8) 466.8.

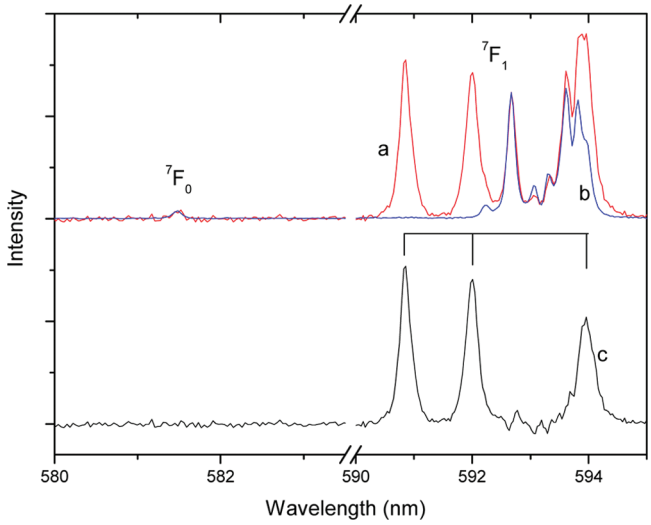

Figure 5. Site-selective emission spectra of YBO_3:Eu^{3+} (0.5 atom %) at 10 K on arbitrary scales excited by (a) 460.3 nm, (b) 465.95 nm, and (c) subtracted spectrum derived by a − b. The terminal states are labeled in a. Spectra a and b are normalized on the bands at 592.67 nm. Note the scale break between 583.5 and 590 nm, where no spectral features are observed.

the transition $^5D_0 \rightarrow {}^7F_0$ is not observed. This spectral behavior is typical for a Eu^{3+} ion at a C_i site, and moreover, there are no other $^5D_0 \rightarrow {}^7F_J$ bands observed in the spectrum. The subtraction of Figure 6a and 6b gives Figure 6c. One $^5D_0 \rightarrow {}^7F_0$ zero-phonon line and three strong $^5D_0 \rightarrow {}^7F_1$ bands are observed in Figure 6c, and as mentioned above, the remainder of the $^5D_0 \rightarrow {}^7F_J$ bands may be assigned to an Eu^{3+} ion situated at one C_1 site. The spectral assignments therefore place the location of Eu^{3+} ions at C_1 and C_i sites, which is consistent with the $C2/c$ space group of YBO_3 (Table 1).

Finally, four weaker bands are apparent in the spectrum of Figure 6c, and these are located (in cm^{-1}) at 313, 337, 344, and 364 to low energy of the $^5D_0 \rightarrow {}^7F_0$ zero-phonon line of the C_1 site. The relative intensities of these bands are reasonably constant with respect to the three strong bands of the C_1 site. There are several possible assignments for these bands. First, they could correspond to Eu^{3+} ions at two minority sites; second, they may correspond to Eu^{3+} ions at one minority site together

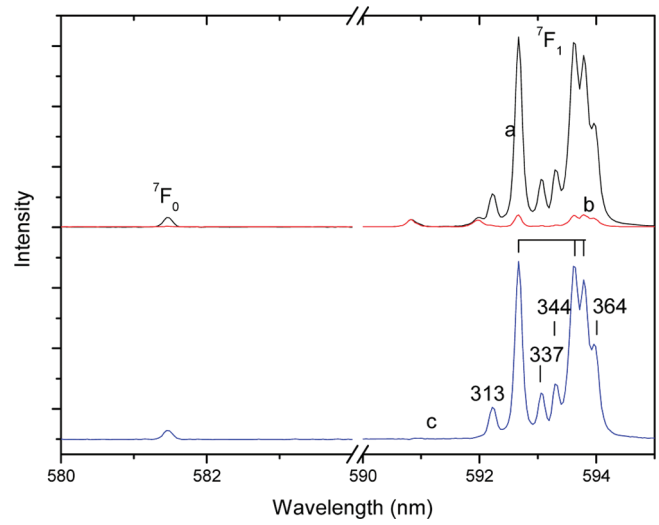

Figure 6. Site-selective emission spectra of YBO_3:Eu^{3+} (0.5 atom %) at 10 K on arbitrary scales excited by (a) 466.1 nm, (b) 462.8 nm, and (c) subtracted spectrum derived by a − b. The terminal states are labeled in a. The spectra a and b are normalized on the bands at 590.82 nm. Note the break in the scale between 584 and 590 nm where no spectral features are observed. Displacements of weak structure from the $^5D_0 \rightarrow {}^7F_0$ zero phonon line are marked in cm^{-1}.

with phonon-coupled modes; and third, these bands could be associated entirely with phonon-coupled modes of the $^5D_0 \rightarrow {}^7F_0$ transition. If these bands in the luminescence spectra correspond to local modes of the Eu^{3+} ion, the corresponding frequencies are not necessarily present in the vibrational spectrum of the host. The observation of phonon structure for the $^5D_0 \rightarrow {}^7F_0$ transition is not unusual, and in other studies, vibronic bands have previously been reported for this transition in the low-temperature emission spectra of moieties with Eu−O bonds.[21–23] There is no indication of minority sites in the absorption spectra subsequently referred to so that the detailed assignment of these weaker bands is not considered further.

In order to strengthen the interpretation given above, the 10 K visible electronic absorption spectrum of YBO_3:Eu^{3+} (5 atom %) was recorded (Figure 7) and consistently interpreted. The absorption spectrum monitors the bulk sample so that trace impurities or defect sites exhibit only minor intensity. At 10 K, absorption takes place from the ground-state level of $^7F_0$ and for the transitions to ^5D_J ($J = 0-2$) only the magnetic dipole transition to $^5D_1$ is expected to be observed for both the C_1 and C_i sites. Forced electric dipole transitions from $^7F_0$ are only active for the Eu^{3+} ion at the C_1 site. These considerations are exemplified by the observation of 1 and 5 bands for $^7F_0 \rightarrow {}^5D_0$ (Figure 7b) and $^7F_0 \rightarrow {}^5D_2$ (Figure 7a), respectively, whereas 6 overlapping bands (as marked in the figure) can be inferred in the transition $^7F_0 \rightarrow {}^5D_1$, Figure 7c. There is only one feature in the $^7F_0 \rightarrow {}^5D_0$ spectral region, as compared to the three zero-phonon lines reported by Boyer et al.[1,24] and Wei et al.[15] Figure 7d shows the longer wavelength part of the absorption spectrum and is in fact the $^5D_0 \rightarrow {}^7F_1$ emission spectrum with nonselective excitation by the tungsten lamp. The relative intensities of the C_1 and C_i site bands are fairly similar to those in Figure 4 under shorter wavelength excitations.

Crystal-Field Calculations. Structural data[9] show that for both sites, Eu^{3+} is surrounded by 8 oxygen atoms which form a distorted cubic environment. Nearly all of the C_i energy levels cannot be determined from the electronic spectra because the associated transitions are silent. The energy level parametrization is therefore mostly limited to the levels of the C_1 site. Although

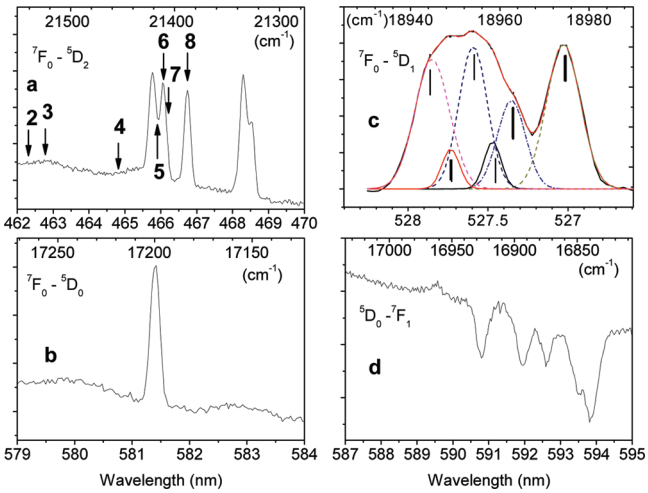

Figure 7. 10 K electronic absorption spectra of a powder sample of $YBO_3:Eu^{3+}$ (5 atom %) at 10 K. The ordinate is absorption (arbitrary units). The last panel shows that emission, rather than absorption, was recorded in the spectral region 590.5−595 nm. A baseline has been constructed in Figure 7c, and the structure has been decomposed into six Gaussian peaks centered (in cm^{-1}) at 18 945 (C_1), 18 949 (C_i), 18 954 (C_1), 18 958 (C_1), 18 963 (C_i), and 18 974 (C_i) cm^{-1} with the tentative assignments of the Eu^{3+} sites based upon crystal-field calculations. The locations of the C_i (C_1) site bands are marked by thick (thin) lines in the figure. The excitation wavelengths utilized in Figure 4 (labeled 2−8) are marked in Figure 7a.

the exact site symmetry of Eu^{3+} is only C_1 for this site, some assumptions and simplifications have been made in minimizing the number (27) of crystal-field parameters required for an energy level analysis. Herein the one-electron crystal-field interaction is included in the electronic energy level calculation, and the empirical Hamiltonian can be written as in descending symmetry order in standard notation[25] as

$$H = E_{avg} + \sum_{k=2,4,6} F^k \mathbf{f}_k + \zeta_{4f} \sum_{i=1}^{6} \mathbf{s}_i \cdot \mathbf{l}_i \quad (1a)$$

$$+ \sum_{k=2-4,6-8} T^k \mathbf{t}_k(\mathrm{f}) + \alpha \mathbf{L}^2(\mathrm{f}) + \beta \mathbf{G}(G_2(\mathrm{f})) + \gamma \mathbf{G}(G_7(\mathrm{f})) \quad (1b)$$

$$+ \sum_{k=0,2,4} M^k \mathbf{m}_k(\mathrm{f}) + \sum_{k=2,4,6} P^k \mathbf{p}_k(\mathrm{f}) \quad (1c)$$

$$+B_C^4\left[\mathbf{C}_0^{(4)} + \sqrt{\frac{5}{14}}(\mathbf{C}_4^{(4)} + \mathbf{C}_{-4}^{(4)})\right] + B_C^6\left[\mathbf{C}_0^{(6)} - \sqrt{\frac{7}{2}}(\mathbf{C}_4^{(6)} + \mathbf{C}_{-4}^{(6)})\right] \quad (1d)$$

$$+B_0^2\mathbf{C}_0^{(2)} + B_2^2(\mathbf{C}_2^{(2)} + \mathbf{C}_{-2}^{(2)}) \quad (1e)$$

$$+B_{D4}^4\left[\mathbf{C}_0^{(4)} - \sqrt{\frac{7}{10}}(\mathbf{C}_4^{(4)} + \mathbf{C}_{-4}^{(4)})\right] + B_2^4\mathbf{C}_2^{(4)} \quad (1f)$$

$$+B_{D4}^6\left[\mathbf{C}_0^{(6)} - \sqrt{\frac{1}{14}}(\mathbf{C}_4^{(6)} + \mathbf{C}_{-4}^{(6)})\right] + B_2^6(\mathbf{C}_2^{(6)} + \mathbf{C}_{-2}^{(6)}) + B_6^6(\mathbf{C}_6^{(6)} + \mathbf{C}_6^{(6)}) \quad (1g)$$

$$+H_{cf}(C_1) \quad (1h)$$

Here eqs 1a−1c represent the quasi-free-ion Hamiltonian for Eu^{3+} with parameters that vary only slightly with different hosts.[25] Equation 1d shows the dominant crystal-field interactions in cubic symmetry. Terms 1e−1g are additional terms required for C_{2v} symmetry. For the approximate analysis, the splitting of $^7F_1$ and $^5D_1$ can be completely described by term 1e, while 1e and 1f are required by $^7F_2$ and $^5D_2$, and 1e−1g are required by $^7F_{3-6}$ and $^5D_3$. Term 1h contains all additional parameters for C_1 symmetry, which is considered as a smaller perturbation here.

TABLE 2: Optimized Parameters for Eu^{3+} at the C_1 Site Using the Descending Symmetry Method[a]

parameter	value	δ
E_{AVG}	63 651	32
F^2	82 577	42
ζ	1333	4
α	20	
β	−617	
γ	1460	
T^2	370	
T^3	40	
T^4	40	
T^6	−330	
T^7	380	
T^8	370	
M^0	2.4	
P^2	303	
B_0^2	−148	76
B_2^2	4	54
B_2^4	−346	67
B_C^4	−2023	54
B_C^6	456	33
B_{D4}^4	−62	104
N_E	28	
N_p	7	
σ	21.5	

[a] B_0^2 and B_2^2 were optimized by being held fixed in the final optimization; $F^4/F^2 = 0.7175$, $F^6/F^2 = 0.5151$, $M^2/M^0 = 0.56$, $M^4/M^0 = 0.38$, $P^4/P^2 = 0.75$, and $P^6/P^2 = 0.5$ were used to constrain those parameters not listed in the table. N_E and N_p are the number of levels fitted and the number of freely-adjustable parameters. $\sigma = [\sum_{i=1,\ldots,N_E}(E_i(\mathrm{calcd}) - E_i(\mathrm{expt}))^2/(N_E - N_p)]^{1/2}$. δ is the parameter standard deviation. The units are cm^{-1}.

The measured levels cover only two spectral multiplet terms, ^7F and ^5D, so that only one of F^k ($k = 2, 4,6$) was varied, and the F^4/F^2 and F^6/F^2 ratios calculated from mean values for Eu^{3+} in crystals were employed.[25] The parameter for the spin−orbit interaction was also freely varied. Other quasi-free-ion parameters in 1b and 1c were held fixed to the mean values for Eu^{3+}. The cubic crystal-field parameters B_C^4 and B_C^6 were treated as free-varying parameters, with B_C^4 being constrained mainly by the splitting of $^7F_2$ and $^5D_2$ into (two) E levels and (three) T_2 levels. B_0^2 and B_2^2 were determined by the splitting of the $^7F_1$ and $^5D_1$ multiplets. Then B_{D4}^4 and B_2^4 were added for the splitting of E and T_2 levels for $^7F_2$ and $^5D_2$. The incompleteness of $^7F_3$ and $^7F_4$ levels did not allow for a complete determination of the comparatively smaller rank-6 parameters, and so that only B_C^6 was included in the fitting.

Table 2 summarizes the parameter values, and the observed energies of crystal-field levels of Eu^{3+} at the C_1 site are compared with the calculated values in Table 3.

For the C_i site, only the relative energies of three levels of $^7F_1$ were experimentally determined from the $^5D_0$ emission spectrum, from which the two crystal-field parameters $B_0^2 = -295$ cm^{-1} and $B_2^2 = 157$ cm^{-1} were determined and $F^2 = 82725$ cm^{-1} by using the spin−orbit coupling parameter, ζ, with the same value as at the C_1 site. The overall strength of the rank-2 parameters ($\sqrt{|B_0^2|^2 + 2|B_2^2|^2}$) for the C_i site is 2.25 times of that for the C_1 site. Notice that this crystal-field strength is a longer range ($1/R^3$) probe and not largely determined by the

TABLE 3: Measured (expt) and Calculated (calcd) Energy Levels of Eu^{3+} in YBO_3:Eu^{3+} (units, cm^{-1}) and Their Deviations (Δ, cm^{-1}) for the C_1 site[a]

level no.	^{2S+1}L	J	expt C_1 site	calcd C_1 site	Δ
1	7F	0	0	−15	−15
2	7F	1	325	324	−1
3	7F	1	352	351	−1
4	7F	1	357	356	−1
5	7F	2	803	791	−12
6	7F	2	825	832	7
7	7F	2	857	845	−12
8	7F	2	1244	1254	10
9	7F	2	1280	1316	36
10	7F	3	1796	1839	43
11	7F	3	1859	1862	3
12	7F	3	1891	1876	−15
13	7F	3	1944	1946	2
14	7F	3		1988	
15	7F	3	2000	2006	6
16	7F	3	2139	2116	−23
17	7F	4	2466	2472	6
18	7F	4	2776	2784	8
19	7F	4		2810	
20	7F	4	2893	2874	−19
21	7F	4	2995	2979	−16
22	7F	4	3055	3078	23
23	7F	4	3099	3118	19
24	7F	4		3124	
25	7F	4	3190	3141	−49
50	5D	0	17 198	17 194	−4
51	5D	1	*18 944*	18 933	−11
52	5D	1	*18 954*	18 944	−10
53	5D	1	*18 958*	18 948	−10
54	5D	2	21 343	21 353	10
55	5D	2	21 354	21 371	17
56	5D	2	21 425	21 436	11
57	5D	2	21 456	21 443	−13
58	5D	2	21 470	21 450	−20
59	5D	3		24 261	
60	5D	3		24 266	
61	5D	3		24 274	
62	5D	3		24 278	
63	5D	3		24 302	
64	5D	3		24 309	
65	5D	3		24 313	

no.	^{2S+1}L	J	expt C_i site	calcd C_i site
1	7F	0	0	−13
2	7F	1	$E_1 + 320$	307
3	7F	1	$E_1 + 352$	339
4	7F	1	$E_1 + 408$	395
50	5D	0	[17 246]	17 233
51	5D	1	*18 949*	18 965
52	5D	1	*18 963*	18 977
53	5D	1	*18 974*	19 002

[a] The standard deviation is 22 cm^{-1}. The measured energies for the C_i site together with those calculated with the parameter values for ζ, F_2, B_0^2, and B_2^2 are also listed for comparison. The experimental values in italics are tentative assignments from the fitting of Figure 7c and were not used in the optimization of parameters. For the C_i site, the absolute value (cm^{-1}) of the lowest $^7F_1$ crystal-field level, $E_1 + 320$ (where E_1 is unknown), was not given experimentally but was set at 320 cm^{-1} to match the predicted splitting. The value of $^5D_0$ is 17 246 cm^{-1} when E_1 is set to zero.

nearest-neighbor oxygen distances for which the mean values at the C_1 and C_i sites are 235.6 and 238 pm, respectively.[9]

Under the approximation of one-particle crystal-field interaction and neglecting the mixing of multiplets of different J values, the calculated $^5D_1$ splitting will always follow the same pattern as, but only about one-third of, $^7F_1$. This is determined by the ratio of the reduced matrix elements of $\langle {}^5D_1||U^2||{}^5D_1\rangle / \langle {}^7F_1||U^2||{}^7F_1\rangle$ (refer to section 5.7 of ref 25) which is about 1/3 but depends weakly on the quasi-free-ion parameters F^k (k = 2, 4, 6). From previous experimental studies, the ratio of splitting is found to be reduced to around 1/4 (page 223 of ref 25) due to an interaction which tends to reduce the splitting of multiplets of lower spin. The calculation in Table 3 accounts well for the crystal-field splittings of the three closely spaced C_1 site $^5D_1$ levels (which were not fitted), as marked in Figure 7c by thin vertical lines.

The remaining three bands in Figure 7c then correspond to $^7F_0 \rightarrow {}^5D_1$ transitions at the C_i site (marked by thick vertical lines). These levels are identified from the Gaussian curve fitting (Figure 7c) to be at the energies marked in italics in Table 3 for the C_i site. The Gaussian fits were employed because the spectrum of the 5 atom % Eu^{3+} sample is inhomogenously broadened. The ratio of the splittings of the $^5D_1$ and $^7F_1$ levels for the C_i site is then determined as 0.28, which is consistent with the ratio of ~1/4.

An interesting observation concerns the C_1 and C_i site occupations by Eu^{3+} in the rather heavily doped (5 atom %) YBO_3 sample. The site occupation ratio is readily determined from the integrated areas of the $^7F_0 \rightarrow {}^5D_1$ transitions at the two sites (Figure 7c). This gives the measured intensity ratio of the C_1 versus C_i site bands as 1.2:1. This ratio is expected to be near 2:1 for this magnetic dipole-allowed transition (which only acquires a small amount of additional electric dipole intensity at the C_1 site[25]). Thus, the substitution of Y^{3+} by Eu^{3+} is not random at high dopant ion concentrations but shows a preference for the site with longer average metal−ligand distance. The crystallographic data show that the overall range of Y−O bond distances is wider for the C_1 site than the C_i site. The crucial factor for site occupation is that the shortest distance for the C_1 site (222.9 pm) is much shorter than for the C_i site (230.0 pm).[9] Since the VIII ionic radius of Eu^{3+} (106.6 pm) is rather longer than that of Y^{3+} (101.9 nm) there is a slight preference for occupation of the site with the longer metal−ligand distance.

Y_3BO_6:Eu^{3+} Impurity Bands in the Spectrum of YBO_3:Eu^{3+}. The products of the reaction of H_3BO_3 with $Ln(NO_3)_3$ strongly depend on the ratio of the starting materials. Due to the high volatility of H_3BO_3, during the course of reaction the ratio of the starting materials readily deviates from the stoichiometric ratio and therefore parasite phases may appear. Even trace amounts of the parasite phases can greatly complicate the emission spectra and make interpretation unreliable. Herein, the high-resolution emission spectra of YBO_3:Eu^{3+} containing a trace amount of Y_3BO_6 was recorded and compared with the spectra of YBO_3 and Y_3BO_6. This serves as a reference to elucidate the concern on the red/orange color ratio of YBO_3:Eu^{3+} emission.

The emission features of Y_3BO_6:Eu^{3+} in Figure 8c are similar to those reported in Figure 7 of ref 26, which displays the 15 K spectrum of Y_3BO_6:Eu^{3+} (2 atom %) upon $^5D_2$ excitation. Note that the intensity in Y_3BO_6:Eu^{3+} of the red emission $^5D_0 \rightarrow {}^7F_2$ is much stronger than that of the orange emission from $^5D_0 \rightarrow {}^7F_1$. By comparing the emission spectrum in Figure 8b of YBO_3:Eu^{3+} prepared with the stoichiometric amounts of reactants with that in Figure 8a of YBO_3:Eu^{3+}, the locations of the extra bands in Figure 8b, which match well with those in Figure 8c, can be definitely attributed to the emission of Y_3BO_6:Eu^{3+} impurity present in YBO_3:Eu^{3+}. The contamination of Y_3BO_6:Eu^{3+} in YBO_3:Eu^{3+} thus makes the intensity of red emission comparable

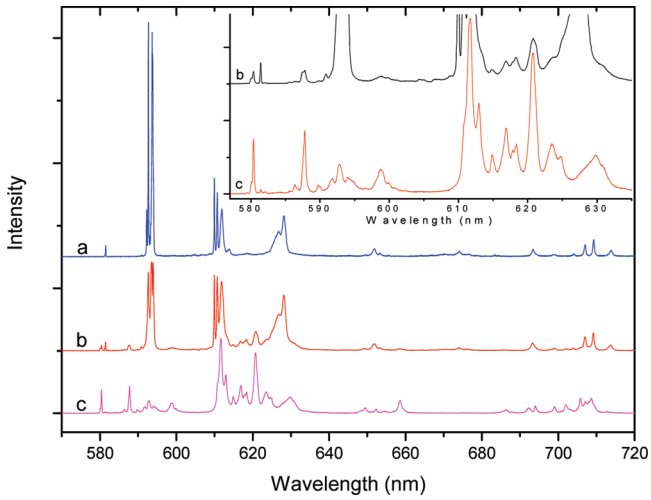

Figure 8. 10 K emission spectra of (a) $YBO_3:Eu^{3+}$ (5 atom %), (b) $YBO_3:Eu^{3+}$ (5 atom %) plus a trace amount of Y_3BO_6, as prepared using H_3BO_3:$Y(NO_3)_3$ reactants in a 1:1 molar ratio, and (c) $Y_3BO_6:Eu^{3+}$ (5 atom %) on arbitrary scales excited by 465.95 nm. The intensity of the $^5D_0 \rightarrow {}^7F_1$ transition in Figure 8b has been truncated. The inset shows a scale expansion.

with that of orange emission and could therefore be purposely employed to tune the phosphor color.

Conclusions

The techniques of FT-IR and XRD are not determinative on the crystal structure of YBO_3. However, the use of Eu^{3+} as a luminescence probe enables a distinction to be made between the various proposed crystal structures. Under the excitation into the $^5D_2$ multiplet term, the bands in the $^5D_0 \rightarrow {}^7F_1$ transition exhibit both relative and absolute variable intensity with selective laser excitation. Higher energy excitation into $^5D_2$, presumably into the very weak $^5D_0 \rightarrow {}^7F_2$ vibronic side band of the C_i site, leads to very weak emission with bands due to the C_i site being dominant. Lower energy selective excitation into $^5D_2$ favors the C_1 site emission. However, complete site selection was not achieved in these spectra, so that the emission spectrum of a certain distinct site was derived by normalization and subtraction. The number of bands in the $^5D_0 \rightarrow {}^7F_J$ emission spectrum at 10 K and the 10 K $^7F_0 \rightarrow {}^5D_J$ absorption spectrum were consistent with the assignment of Eu^{3+} ions at C_1 and C_i sites. In particular, the ions at the C_i site are silent except for the $^5D_0 \rightarrow {}^7F_1$ and $^7F_0 \rightarrow {}^5D_1$ magnetic dipole orbitally-allowed transitions. Both the absorption and derived emission spectral features are therefore in good agreement with the structure determination performed by Lin et al.[9]

Some authors have attributed the reason why $^5D_0 \rightarrow {}^7F_1$ is particularly intense, relative to $^5D_0 \rightarrow {}^7F_2$, in the spectra of $YBO_3:Eu^{3+}$ to the near-centrosymmetry of Eu^{3+}. The reason actually stems from the occupation of two distinct sites by Eu^{3+} and the fact that forced electric dipole transitions are forbidden at the C_i site. Thus, this site only contributes intensity in the $^5D_0$ emission spectrum in the transition $^5D_0 \rightarrow {}^7F_1$. All of the other transitions from $^5D_0$ comprise forced electric dipole emission from only one site. Although the site symmetry is C_1, the band splittings (e.g., into pseudo-E and -T levels for $^7F_2$) indicate a fairly small distortion from trigonal symmetry at this site.

Special care should be taken in the preparation of YBO_3 since the product of the reaction strongly depends on the ratio of starting materials. Even a trace amount of the parasite phase of Y_3BO_6 in YBO_3 complicates the Eu^{3+} emission spectra and changes the red/orange color ratio of $YBO_3:Eu^{3+}$ emission.

Acknowledgment. Financial support from the City University of Hong Kong Strategic Research Grant 7002292 is gratefully acknowledged. We acknowledge the funding of travel expenses under the Hong Kong−France Research Grant Fund 9050206.

References and Notes

(1) Boyer, D.; Bertrand-Chadeyron, G.; Mahiou, R.; Caperaa, C.; Cousseins, J.-C. *J. Mater. Chem.* **1999**, *9*, 211.
(2) Heller, G. *Top. Curr. Chem.* **1986**, *131*, 39.
(3) Levin, E. M.; Roth, R. S.; Martin, J. B. *Am. Mineral.* **1961**, *46*, 1030.
(4) Newnham, R. E.; Redman, M. J.; Santoro, R. P. *J. Am. Ceram. Soc.* **1963**, *46*, 253.
(5) Bradley, W. F.; Graf, D. L.; Roth, R. S. *Acta Crystallogr.* **1966**, *20*, 283.
(6) Chadeyron, G.; El-Ghozzi, M.; Mahiou, R.; Arbus, A.; Cousseins, J. C. *J. Solid State Chem.* **1997**, *128*, 261.
(7) Hosokawa, S.; Tanaka, Y.; Iwamoto, S.; Inoue, M. *J. Mater. Sci.* **2008**, *43*, 2276.
(8) Ren, M.; Lin, J. H.; Dong, Y.; Yang, L. Q.; Su, M. Z.; You, L. P. *Chem. Mater.* **1999**, *11*, 1576.
(9) Lin, J. H.; Sheptyakov, D.; Wang, Y. X.; Allenspach, P. *Chem. Mater.* **2004**, *16*, 2418.
(10) Chadeyron, G.; Mahiou, R.; El-Ghozzi, M.; Arbus, A.; Zambon, D.; Cousseins, J. C. *J. Lumin.* **1997**, *564*, 72–74.
(11) Hölsa, J. *Inorg. Chim. Acta* **1987**, *139*, 257.
(12) Bril, A.; Wanmaker, W. L. *J. Electrochem. Soc.* **1964**, *111*, 1363.
(13) Wei, Z.-G.; Sun, L.-D.; Jiang, X.-C.; Liao, C.-S.; Yan, C.-H.; Tao, Y.; Zhang, J.; Hou, T.-D.; Xie, Y.-N. *Chem. Mater.* **2003**, *15*, 3011.
(14) Kim, D.-S.; Lee, R.-Y. *J. Mater. Sci.* **2000**, *35*, 4777.
(15) Wei, Z. G.; Sun, L. D.; Liao, C. S.; Yin, J. L.; Jiang, X. C.; Yan, C. H.; Lu, S. Z. *J. Phys. Chem. B* **2002**, *106*, 10610.
(16) Joffin, N.; Dexpert-Ghys, J.; Verelst, M.; Baret, G.; Garcia, A. *J. Lumin.* **2005**, *113*, 249.
(17) Laperches, J. P.; Tarte, P. *Spectrochim. Acta* **1966**, *22*, 1201.
(18) Denning, J. H.; Ross, S. D. *Spectrochim. Acta A* **1972**, *28*, 1775.
(19) Giesber, H. G.; Ballato, J.; Pennington, W. T.; Kolis, J. W. *Informat. Sci.* **2003**, *149*, 61.
(20) Lin, J. H.; Zhou, S.; Yang, L. Q.; Yao, G. Q.; Su, M. Z.; You, L. P. *J. Solid. State Chem.* **1997**, *134*, 158.
(21) Berry, M. T.; Kirby, A. F.; Richardson, F. S. *Mol. Phys.* **1989**, *66*, 723.
(22) Tanner, P. A.; Pan, Z. *Inorg. Chem.* **2009**, *48*, 11142.
(23) Yamada, N.; Shionoya, S. *J. Phys. Soc. Jpn.* **1971**, *31*, 841.
(24) Boyer, D.; Bertrand, G.; Mahiou, R. *J. Lumin.* **2003**, *104*, 229.
(25) Görller-Walrand, C.; Binnemans, K. *Handbook on the Physics and Chemistry of Rare Earths*; Gschneidner, K. A., Jr., Eyring, L., Eds.; Elsevier Science B.V.: Amsterdam, 1996; Chapter 23, pp 121−283.
(26) Boyer, D.; Bertrand-Chadeyron, G.; Mahiou, R.; Brioude, A.; Mugnier, J. *Opt. Mater.* **2003**, *24*, 35.

JP910329K